

Electron-tomographic analysis of intraflagellar transport particle trains *in situ*

Gaia Pigino,¹ Stefan Geimer,² Salvatore Lanzavecchia,³ Eugenio Paccagnini,¹ Francesca Cantele,³ Dennis R. Diener,⁴ Joel L. Rosenbaum,⁴ and Pietro Lupetti¹

¹Dipartimento di Biologia Evolutiva, Università di Siena, 53100 Siena, Italy

²Zellbiologie/Elektronenmikroskopie, Universität Bayreuth, 95440 Bayreuth, Germany

³Dipartimento di Chimica Strutturale, Università degli Studi di Milano, 20133 Milano, Italy

⁴Department of Molecular, Cellular and Developmental Biology, Yale University, New Haven, CT 06520

Intraflagellar transport (IFT) is the bidirectional movement of multipolypeptide particles between the ciliary membrane and the axonemal microtubules, and is required for the assembly, maintenance, and sensory function of cilia and flagella. In this paper, we present the first high-resolution ultrastructural analysis of trains of flagellar IFT particles, using transmission electron microscopy and electron-tomographic analysis of sections from flat-embedded *Chlamydomonas reinhardtii* cells. Using wild-

type and mutant cells with defects in IFT, we identified two different types of IFT trains: long, narrow trains responsible for anterograde transport; and short, compact trains underlying retrograde IFT. Both types of trains have characteristic repeats and patterns that vary as one sections longitudinally through the trains of particles. The individual IFT particles are highly complex, bridged to each other and to the outer doublet microtubules, and are closely apposed to the inner surface of the flagellar membrane.

Introduction

Intraflagellar transport (IFT) is a motility process that occurs between the flagellar membrane and the axoneme in eukaryotes. It was first observed in the flagella of the biflagellate alga *Chlamydomonas reinhardtii* by differential interference contrast (DIC) microscopy as large, variably sized varicosities moving continuously to the flagellar tip (anterograde) at $\sim 2.0\text{ }\mu\text{m/s}$, and smaller varicosities moving from tip to base (retrograde) at $3.5\text{ }\mu\text{m/s}$ (Kozminski et al., 1993). Transmission electron microscopy (TEM) of thin sections of flagella (Kozminski et al., 1995; Pedersen et al., 2006) showed that these varicosities were underlain by particle trains of varying length and appeared to be associated with the outer doublet microtubules (MTs) by thin connections, and even more closely associated with the inside of the flagellar membrane. The latter association was indicated by the fact that the otherwise loose-appearing flagellar membrane was always tightly applied to the surface of the trains of IFT particles facing the membrane (Kozminski et al., 1993; 1995). These trains of particles between the membrane and the axoneme

were positively identified as IFT particles by immuno-EM using anti-IFT antibodies (Pedersen et al., 2006).

Since the initial observation and identification of IFT in *C. reinhardtii* flagella by DIC and TEM, IFT particle polypeptides have been found in many eukaryotic cilia and flagella (Beech et al., 1996; Cole et al., 1998; Rosenbaum et al., 1999; Pazour et al., 2002; Rosenbaum and Witman, 2002; Scholey, 2003; Sloboda and Howard, 2007; Pedersen and Rosenbaum, 2008), although ultrastructural observations of them have been confined principally to *C. reinhardtii* flagella (Kozminski et al., 1993, 1995; Dentler, 2005; Pedersen et al., 2006). There have been no studies that have focused specifically on the detailed 3D analysis of the trains of IFT particles.

This paper is the first to describe the ultrastructure of the trains of IFT particles using fixed and embedded material that has then been thin- and thick-sectioned for tomographic analysis in the transmission electron microscope. These studies were initiated with the knowledge that the rows of IFT particles were probably highly complex structures, as it had been described that they are required for transporting prefabricated axonemal

G. Pigino and S. Geimer contributed equally to this paper.

Correspondence to Pietro Lupetti: lupetti@unisi.it

Abbreviations used in this paper: DIC, differential interference contrast; IFT, intraflagellar transport; MT, microtubule; TEM, transmission electron microscopy; WT, wild type.

© 2009 Pigino et al. This article is distributed under the terms of an Attribution-Noncommercial-Share Alike-No Mirror Sites license for the first six months after the publication date (see <http://www.jcb.org/misc/terms.shtml>). After six months it is available under a Creative Commons License (Attribution-Noncommercial-Share Alike 3.0 Unported license, as described at <http://creativecommons.org/licenses/by-nc-sa/3.0/>).

parts such as the radial spokes and dynein arms from the cytoplasm to the flagellar tip for assembly (Rosenbaum and Witman, 2002; Qin et al., 2004; Hou et al., 2007), as well as for movement of axonemal turnover products from the flagellar tip back to the cytoplasm (Marshall and Rosenbaum, 2001; Qin et al., 2004). In addition, kinesin-2-powered anterograde IFT was shown to carry the presumably inactive cytoplasmic dynein 1b to the tip, where it becomes engaged for the retrograde IFT trip back to the cytoplasm, now carrying the inactive kinesin-2 (Pazour et al., 1998, 1999, 2000; Orozco et al., 1999; Signor et al., 1999; Iomini et al., 2001). Finally, the IFT system, in addition to carrying axonemal proteins, is also responsible for the lateral movement of integral membrane polypeptides back and forth along the length of the flagella in the plane of the flagellar membrane bilayer (Qin et al., 2005; Huang et al., 2007). In spite of the presumed complexity of the IFT trains, repeating structures have already been observed in the few electron micrographs of IFT particles *in situ* that have been published (Kozminski et al., 1993, 1995; Dentler, 2005; Pedersen et al., 2006). Moreover, because the polypeptides composing isolated IFT particles sediment in discrete peaks at 16–17S in sucrose gradients (Cole et al., 1998), and because these particles in turn compose the IFT trains (Kozminski et al., 1995), one therefore might expect to find structures of a regular size and periodicity in the IFT trains located between the doublet MTs and the flagellar membrane.

In this paper, we describe our observations on the 3D structure of trains of anterograde and retrograde IFT particles *in situ* by use of electron tomography of sectioned flat-embedded *C. reinhardtii* flagella. In addition, we provide the first evidence for ultrastructural differences between the anterograde and retrograde IFT trains.

Results

Trains of IFT particles can be observed in flagella of sedimented, randomly sectioned, whole *C. reinhardtii* cells, but it is more efficient to use flat-embedded *C. reinhardtii* cells. *C. reinhardtii* can attach to a coverslip by their flagella and undergo gliding motility (Bloodgood, 1981); when fixed and embedded in this position, one can obtain serial longitudinal sections through many flagella in a single area (Fig. 1 a). If, instead, the flat-embedded material is repositioned at 90° to the knife, serial cross sections of the flagella and IFT trains can be obtained (Fig. 1 b).

2D analysis

IFT trains in longitudinal sections of wild-type (WT) flagella. Thin (~60 nm) longitudinal sections of flat-embedded flagella, from WT cells, show trains of IFT particles located in the space between the flagellar membrane and the outer axonemal doublets (Figs. 1 c and 2). The trains appear as electron-opaque structures with an intrinsic repeat of particles. These repeats were previously observed in EM studies of longitudinal sections of *C. reinhardtii* flagella (Kozminski et al., 1993, 1995; Dentler, 2005; Pedersen et al., 2006), although the periodicities have not been measured. Depending on the level

at which the IFT trains are sectioned, it is possible to observe connections linking IFT trains to both the outer doublet MTs and the flagellar membrane (Fig. 2). The links between the IFT train and the outer doublet MTs may represent the molecular motors (kinesin-2 and cytoplasmic dynein 1b) responsible for the movement of the trains. In the absence of IFT complexes, the flagellar membrane appears loosely associated with the underlying axoneme (Fig. 2 g); when an IFT train is present, the membrane always appears to be tightly associated with the IFT train all along its length (Figs. 1 c and 2), with a mean of 37.5 nm between the membrane and the axonemal MTs.

A careful analysis of many thin longitudinal sections of flagella from WT cells clearly revealed the occurrence of two distinct categories of IFT trains (Figs. 1 c and 2): short, thick, electron-opaque trains; and long, thin, less opaque trains. When the lengths of trains that were clearly contained in a single section were measured, they formed two peaks with mean lengths of 250 nm and 700 nm (Fig. 3, a and b). In reviewing the micrographs from which the trains were measured, those trains that clustered around 250 nm were all of the electron-opaque type, with a unit periodicity of ~16 nm, as shown in Fig. 2 (a–e). The periodicities were determined by measuring the total length of each IFT train and dividing by the number of units in the train minus one. These “short” trains were the ones first identified by Ringo (1967) and later noted by others after the discovery of IFT (Kozminski et al., 1993, 1995). The trains whose lengths were 500 nm or more were all of the less electron-opaque type, with a periodicity of ~40 nm, as seen in Fig. 2 (f–l). Based on this morphology, there are two categories of IFT trains that presumably have a different composition or function in the flagellum.

Determination of the number of IFT trains per flagellum. Using standard TEM on serial sections (section thickness of ~40 nm) of flat-embedded WT *C. reinhardtii* cells, the IFT trains were counted in seven flagella that were sectioned longitudinally along almost their entire length, (see Fig. S1 and Table S1). The mean number of IFT trains in a flagellum was 18.1 (SD 5.6), with numbers ranging from 12 to 27 IFT trains. The determined numbers of IFT trains per flagellum are almost certainly underestimated, as the long trains, in particular, tend to go in and out of the plane of sectioning and therefore are difficult to quantify.

***fla14* mutant analysis permits selective observation of anterograde IFT trains.** The *fla14* *C. reinhardtii* mutant is characterized by the deletion of the LC8 gene, a component of both flagellar (Piperno and Luck, 1979) and cytoplasmic dyneins (King et al., 1996). Although deletion of the LC8 gene does not affect cell growth or cell morphology, and the LC8 gene product is not required for essential cellular process in *C. reinhardtii* (Pazour et al., 1998), the flagella of *fla14* are immotile, approximately half length, with missing or defective radial spokes, and the outer and inner dynein arms are reduced in number (Pazour et al., 1998). Because the deletion of LC8 disrupts the molecular motor for retrograde IFT (dynein 1b), retrograde IFT movement is missing in *fla14* cells, whereas the kinesin-powered anterograde IFT is normal (Pazour et al., 1998). Most importantly,

Wild-Type cells

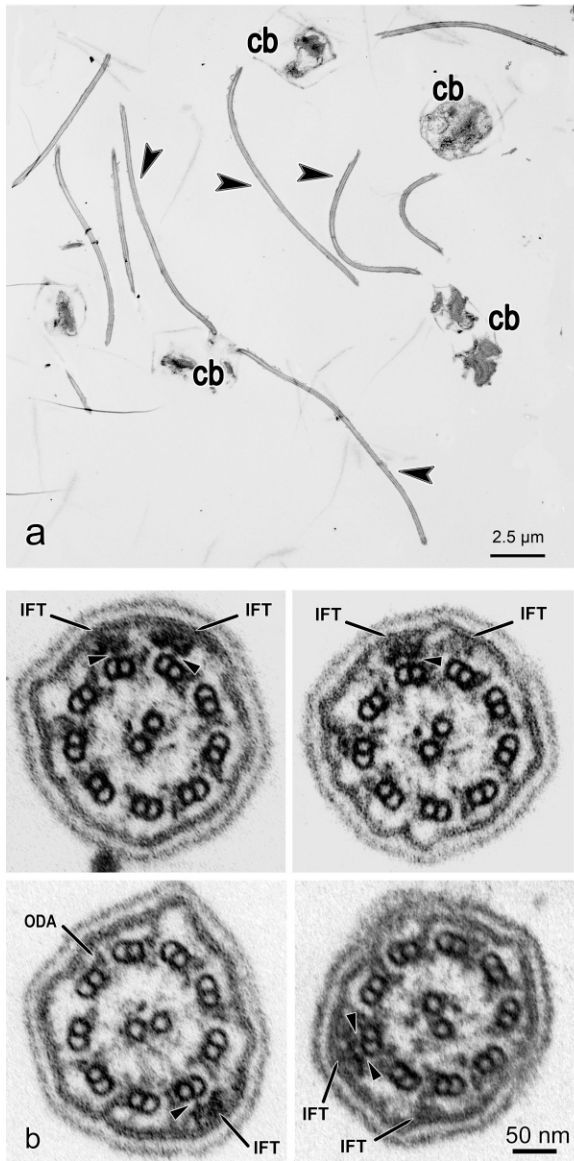
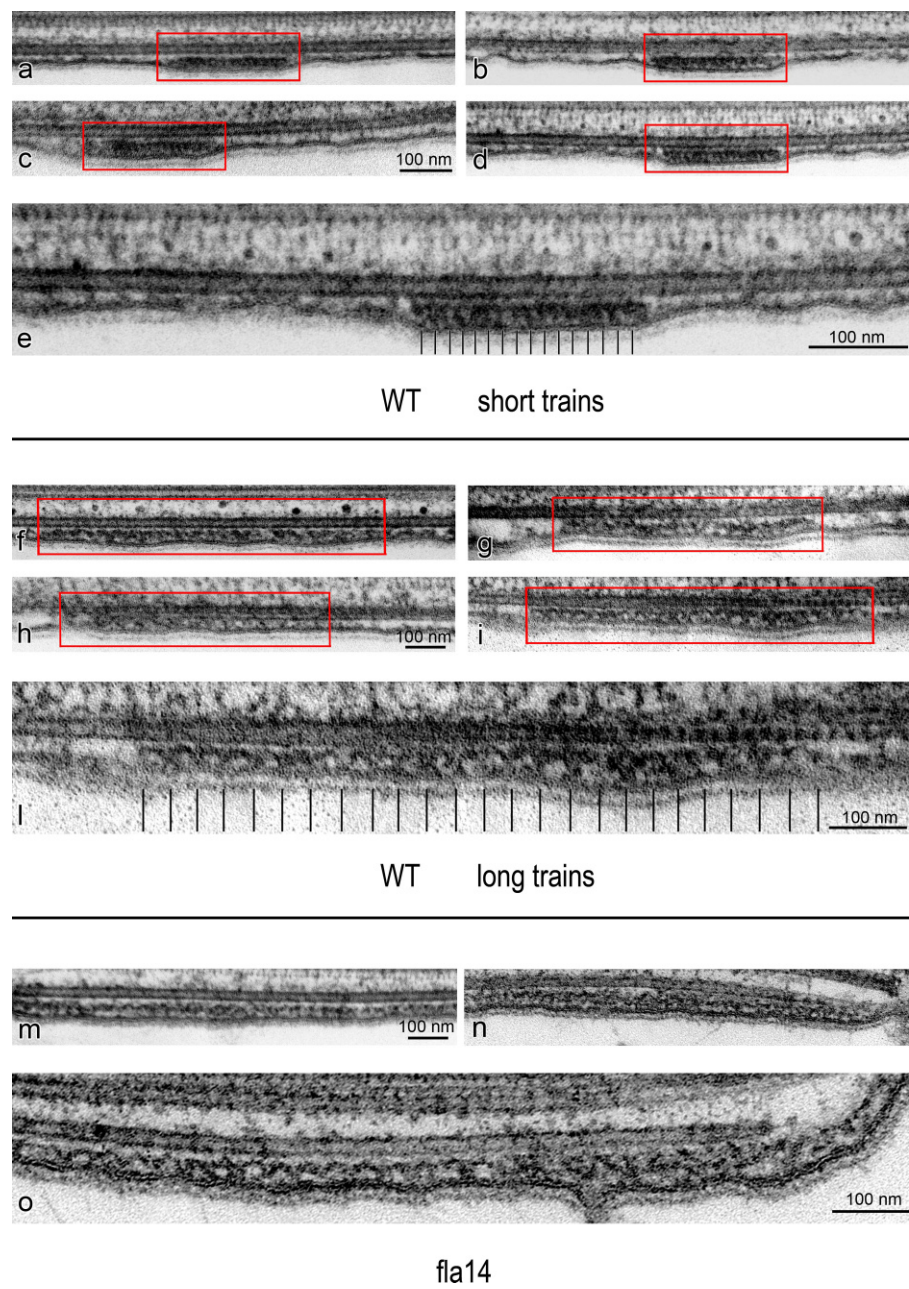


Figure 1. TEM micrographs of flat-embedded flagella from WT *C. reinhardtii* cells containing IFT trains. (a) Low-magnification view of longitudinally sectioned flagella (arrowheads) and cell bodies (cb). (b) Four cross sections of WT flagella containing IFT trains. The arrows show some cross-sectioned IFT trains (IFT), located between the flagellar membrane and the axoneme and close to outer dynein arms (ODA). Arrowheads indicate the links between the IFT trains and B tubule of MT doublets. (c) A longitudinal section of a flat-embedded flagellum from a WT cell. The section is cut through the central core of the flagellum at the level of the central pair apparatus (cp). Two of the nine MT doublets (md) are visible beside the central pair. Underneath the flagellar membrane (m), IFT trains with two different morphologies are present: short trains are labeled with white arrowheads, whereas longer trains are marked with black arrowheads, and their extremities delineated with short black lines.

flagella of *fla14* contain 10–20-fold the amount of IFT particle polypeptides found in WT (Pazour et al., 1998), and, unlike flagella of WT cells, only anterograde IFT occurs. Flagella from *fla14* cells therefore constitute excellent material for studying the structure of anterograde IFT trains by electron tomography. Many nearly identical particles can be sampled from a single tomogram, so this material is also suitable for the study of anterograde IFT particle/train structure by particle-averaging strategies.

The analysis of many longitudinal sections of *fla14* flagella showed that IFT trains very similar to the ones identified as long trains in WT cells were abundant in this mutant. In >150 longitudinal sections of *fla14* flagella analyzed, we observed 700 sections of IFT trains (Fig. 3 a). All of these were of low electron density and/or had the 40-nm periodicity characteristic of long trains in WT flagella (compare Fig. 2, f–l, with Fig. 2, m–o; and see Fig. S2). Only 71 of these trains appeared to be contained completely in a single section, and so were

Figure 2. TEM micrographs of *in situ* IFT trains in flat-embedded flagella from WT and *fla14* mutant cells of *C. reinhardtii*. WT flagella display two types of trains, each with a characteristic length and ultrastructure. (a–d) Four short IFT trains (framed in red lines). (e) A magnified view of panel d showing that these trains are electron dense and compact, with an internal 16-nm repeat of small “lollipop-like particles.” (f–i) Four long IFT trains (framed in red lines). At higher magnification (l), these trains are less compact than short trains and are characterized by an arc-shaped pattern, not seen in short trains. (m, n, and o) Three long IFT trains from *fla14* mutant cells, which lack retrograde IFT. These trains are characterized by a structure and a repeat very similar to those observed in long trains from WT cells.



measured. The mean length of these trains was 755 nm with a standard deviation of 139 nm (Fig. 3, b and c). None of the short, electron-dense trains were observed in these sections. In contrast, 110 longitudinal sections of flagella from WT cells contained 102 short trains (Fig. 3 a). The overall results of the comparative analysis of WT and *fla14* trains support the conclusion that the short, compact, electron opaque trains, absent in the retrograde mutant, are responsible for retrograde IFT, whereas the longer and less compact trains found in both *fla14* and WT flagella underlie anterograde IFT.

IFT trains in cross sections of WT and *pf28* flagella. TEM analyses of thin (~60 nm) cross sections from WT flagella confirmed the presence of IFT particles located between the MT doublets and the flagellar membrane (Fig. 1 b), as previously shown (Kozminski et al., 1993; Pazour et al., 1998).

In WT flagella, outer dynein arms and IFT particles are often seen contacting each other, sometimes making the identification of IFT particles difficult (Fig. 1 b). To overcome this problem, we analyzed cross sections from flagella of the *pf28* mutant, which is missing outer dynein arms (Fig. 4, a–g). The cross-section images of both WT and *pf28* flagella show IFT particles connected to the B subfiber of the doublet by one or two links, and also connected to the flagellar membrane (Figs. 1 b and 4, a–g). The analysis of serial cross sections from *pf28* flagella also revealed that neighboring trains, visible as separate entities (Fig. 4 f), sometimes contact each other, appearing as a single structure with a wider cross section extending over two sets of MT doublets (Fig. 4 g). Because it is known that IFT trains carry cargo, one might expect to see evidence of cargo in cross sections; however, no consistent placement of electron-opaque

material that might be cargo was observed near the IFT particles, and, without specific labeling, we would be unable to identify such cargo.

3D analysis

Electron tomographic analysis of IFT trains from thick sections. We reconstructed several 3D maps from thick sections (~ 100 nm) of flagella of *fla14* cells. The flagella of this retrograde IFT mutant are filled with long IFT trains, many in the proper location bounded by outer doublets and the flagellar membrane. Other trains overlap, forming bulges filled with multiple IFT trains between the flagellar membrane and axoneme (Fig. 5, a and b; Pazour et al., 1998). On the basis of ultrastructure and periodicity, these long trains, whether in the bulges or not, appear to be identical.

Fig. 5 is a montage of tomographic sections from the most informative areas we identified. Fig. 5 (a and b) was obtained by combining 20 contiguous individual (0.66 nm thick) planes from the middle of a tomogram to form virtual, 13.2-nm thick, sections. In the upper part of Fig. 5 a, two long trains of IFT particles are visible between the flagellar membrane and the MT doublets. One IFT train from this tomogram measured ~ 750 nm \times 80 nm \times 25 nm. Links between the IFT particles and the membrane (Fig. 5, a and b, black arrowheads) are shown as well as connections to the MT doublet (Fig. 5, a and b, white arrowheads). The shape and the position of the particles confers a wavelike pattern to the train that is present in almost all the longitudinal planes of the tomogram containing the long IFT trains. Video 1 shows the tomographic reconstruction in Fig. 5 a. We further studied the ultrastructure of IFT trains by analyzing individual planes of several tomograms from *fla14* flagella oriented as in Fig. 5 (a and b). These views confirmed the wavelike pattern seen in IFT trains and afforded a better image of the associations of IFT particles with the flagellar membrane and MT doublets (Fig. 5, c–f). The mean spacing of these links to the MT, measured in 71 areas from three tomograms, was 41.4 nm (SD 2.5).

In the bulges of *fla14* flagella, where IFT trains accumulate between the membrane and the axoneme, some trains maintain their association with MT doublets (Fig. 5, a and b, white arrowheads), and others with the flagellar membrane (Fig. 5, a and b, black arrowheads); these associations appear to be mediated by typical IFT train–MT or train–membrane links, respectively. In the core of a bulge, lines of particles constituting IFT trains are less discernible but are still visible (Fig. 5 b, circled areas), despite having lost their connections with both the flagellar membrane and MTs (Fig. 5, a, b, and f). This indicates that there are connections that link individual IFT particles together, stabilizing the IFT train even in the absence of interactions with the flagellar membrane or axoneme.

The encircled area in the inset between Fig. 5, panels a and b, indicates how volumes have been selected for particle averaging from the tomogram so that each volume contains three contiguous IFT particles with a portion of the flagellar membrane on one side and a tract of the MT doublet on the opposite side. We picked these individual volumes within a single train based on the clarity and ease of detection of the individual IFT units.

Strain	Flagella Assayed	Distinct Long Trains		Distinct Short Trains	
		Total Observed	Total Observed	Total Observed	Total Observed
WT	110	29/82		102/157	
<i>fla14</i>	150	71/700		0/0	

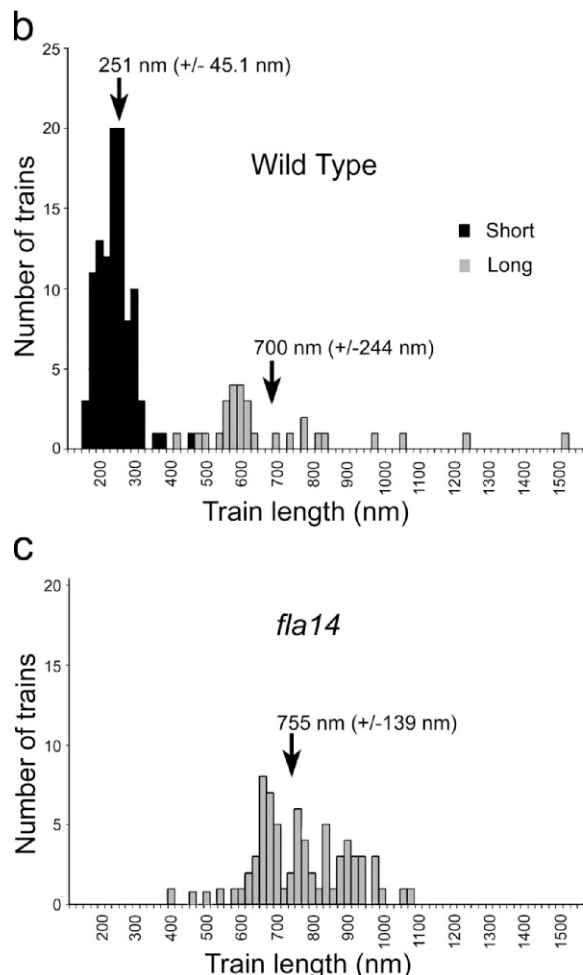


Figure 3. Length distribution of IFT trains in WT and *fla14* flagella. (a) Table of the number of clearly identifiable and measurable long and short IFT trains in WT and *fla14* flagella. (b and c) Histograms of the length distributions of IFT trains in flagella of WT (b) and *fla14* (c) cells. The arrows mark the mean length (\pm SD) of the long (grey) and short (black) IFT trains.

Fig. 6 shows the images that result from serial sectioning along the z axis of a volume reconstructed by averaging 15 individual volumes from within the same train, with each single volume containing one set of three contiguous IFT particles like those shown in Fig. 5 a (inset). This kind of rendering revealed that the IFT structure presents patterning variations depending on the sectioning level of the 3D density map. Panels 1 and 6 (Fig. 6), corresponding to the top and the bottom sections of the IFT train, respectively, show the connections between adjacent IFT particles and the links to the flagellar membrane. In panels 2 and 5 (Fig. 6), each particle appears to be formed of two separate oblong and spherical profiles that alternate to form the IFT train. In panels 3 and 4 (Fig. 6), the three IFT particles show

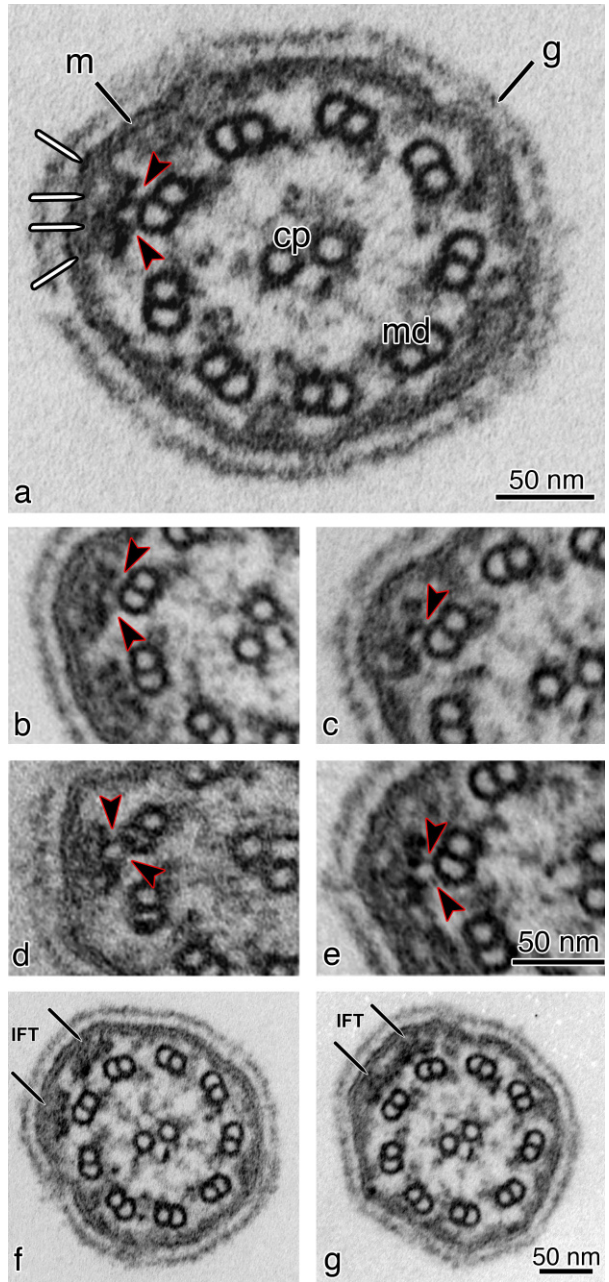


Figure 4. TEM images of cross sections of flagella from flat-embedded *pf28* mutant *C. reinhardtii* cells, which lack outer dynein arms. (a) Cross section of *pf28* flagella showing IFT trains located underneath the flagellar membrane (m). The arrowheads indicate the two links connecting the bilobed IFT particle to the B tubule of a MT doublet (md). The same structures can be observed in b–e (arrowheads). The IFT particle also shows links to the flagellar membrane (white lines). cp, central pair; g, glyocalyx (a membrane overlay composed of hydroxyproline-rich glycoproteins, which surrounds the *C. reinhardtii* flagella). (b–e) Cross sections showing bilobed IFT particles. Each IFT particle has connections with the flagellar membrane on one side and connections to the B tubule of the MT doublet on the other side (arrowheads). (f and g) Two consecutive serial cross sections of a flagellum from a *pf28* mutant cell showing two side-by-side IFT trains on adjacent doublet MTs (arrows). (g) Adjacent IFT trains can occasionally contact each other laterally, forming wider structures that can extend for ~70 nm over two neighboring MT doublets.

links to both the membrane and to the B subtubule of the MT doublet. The symmetry seen in each pair of sections suggests that each IFT particle is composed of two similar parts, one on top of the other.

A surface-rendering representation of part of a long IFT train is shown in Fig. 7. The model in Fig. 7 a is oriented like the tomogram section shown in Fig. 5; i.e., a longitudinal view from the top. From this vantage point, it is possible to identify the same wave pattern (highlighted by the white waving frame in Fig. 7 a) shown in Fig. 2 (f–o) and in Fig. 5. In addition, the longitudinal top view shows the links between IFT particles and the flagellar membrane on one side as well as links between IFT trains and the surface of MT doublets. These links are also visible in the cross view shown in Fig. 7 b and in most of the cross sections in Fig. 1 b and Fig. 4 (arrowheads).

In the 3D model, as well as in most of these EM cross sections, the IFT train seems to be built of two rows of similar particles, each connected by at least two links to the membrane, and by one link to the B subtubule of the MT doublet. The lateral view of the IFT trains, looking outward from the axoneme interior (Fig. 7 c), shows the two rows of particles (circles). The similarity between the particles of the two rows is striking and suggests a twofold rotational symmetry; i.e., the lower particle looks like the upper particle rotated 180°. Oblique links (Fig. 7 c, labeled with d) form lateral connections between neighboring particles. A second set of links (Fig. 7 c, labeled with l), oriented parallel to the longitudinal axis of IFT trains, connect adjacent particles. Fig. 7 c also shows a link (Fig. 7 c, labeled with k) of each individual particle to the surface of the MT doublet. Fig. 7 d shows a lateral view of the three pairs of IFT particles, as seen from the exterior of the flagellum. 1, 2, 3, and 4 indicate the contact points between the particles and the flagellar membrane. A video of the surface rendering in Fig. 7 is available online (Video 2). Because we see these connections between the IFT trains and membrane and MTs in raw EM sections, we are convinced that they represent real structures and not artifacts of the filtration procedure.

To support the reliability of our 3D alignment protocol, we have compared virtual sections from a raw unaveraged density map (Fig. 8 a) of an IFT train from *fla14* flagella (Fig. 8, b and d) with virtual sections of an averaged 3D model cut at the same sectioning levels (Fig. 8, c and e).

We sectioned the tomogram along both the yellow and red sectioning planes shown in Fig. 8 a (i.e., parallel to the axoneme). The ~15-nm-thick digital sections obtained, cutting through the longitudinal axis of the IFT train, are shown in Fig. 8 (b and d). The white arrows indicate the 40-nm repeat of IFT particles along the train. At these section levels, the pairs of particles (Fig. 8, b–e, yellow and red masks) appear connected to each other by obliquely oriented bridging domains (Fig. 8, d and e, arrowheads). As expected, sections from both the tomogram and the averaged model display strikingly similar contours.

Short (retrograde) IFT trains in WT flagella. To define the structure of the short, retrograde IFT trains, double tilt tomographic analysis was performed on flat-embedded flagella from both WT and *pf28* outer dynein armless mutant cells. The structure of the short trains is more heterogeneous and

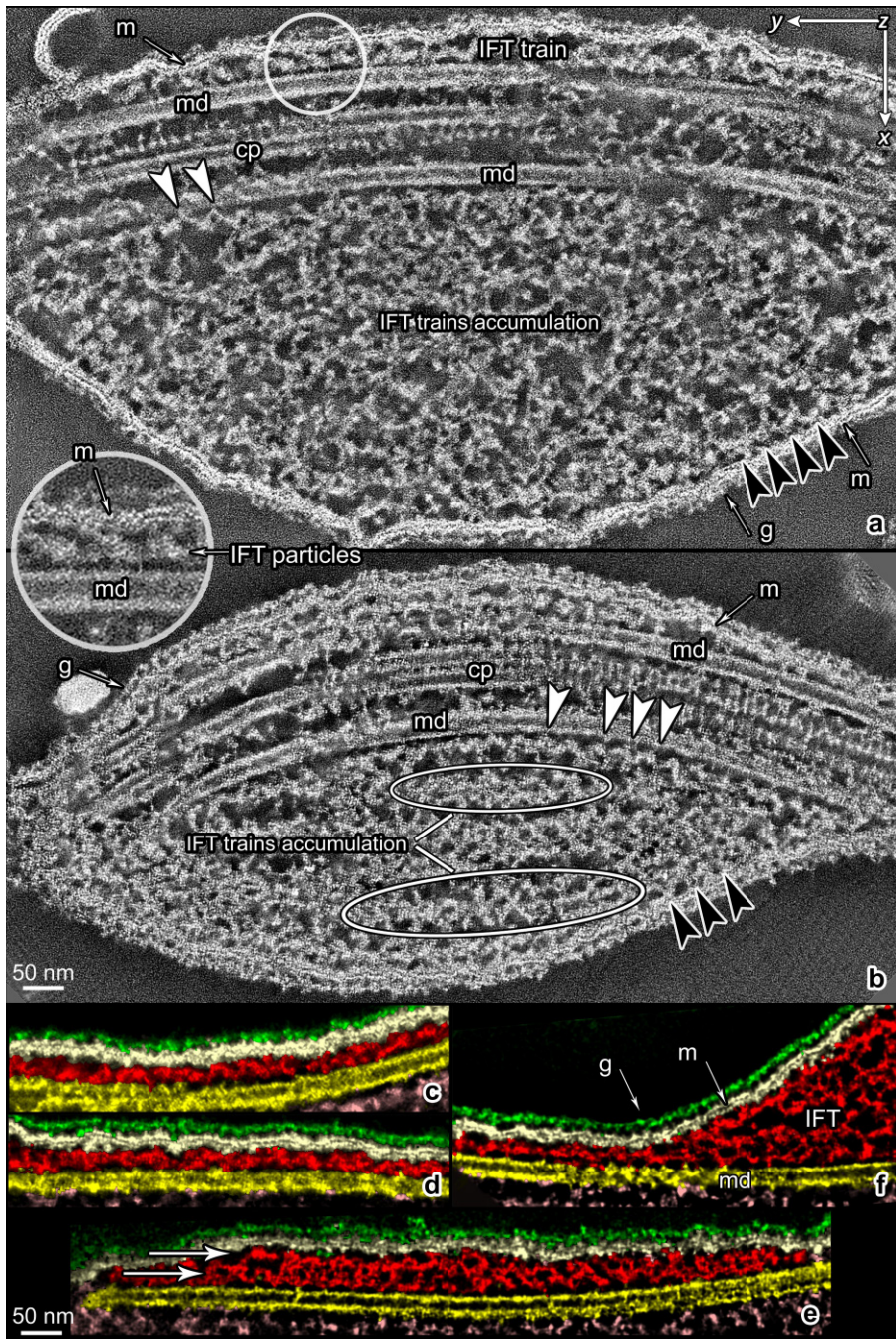


Figure 5. Tomographic sections of flagella from *fla14* mutant *C. reinhardtii*. (a and b) Approximately 13-nm-thick tomographic sections along the central planes of the axonemes. The central pair complex (cp), with its lateral projections, and the MT doublets (md) are visible. In the upper part of the pictures, two long IFT trains are visible in the space between the flagellar membrane (m) and the MT doublets (md). Notice the bulges of IFT trains accumulated in the space between the flagellar membrane and the MT doublets in the bottom part of panels a and b (white ovals), below the axonemes. White arrowheads indicate the links of IFT trains to the MT doublet. Black arrowheads indicate the links between the IFT particles and the flagellar membrane. The white circle in panel a shows one of the zones that has been selected from the tomogram for particle averaging so that each volume contains a tract of the MT doublet, three contiguous IFT particles, and a portion of the flagellar membrane. The inset shows a close up view of the structures in the white circle. Notice the association of IFT particles with the flagellar membrane. g, glycocalyx. (c–f) Montage of 0.66-nm-thick individual planes of tomograms reconstructed from flagella of *fla14* cells. Planes were cut with the same orientation used in panels a and b, and colors were assigned to different flagellar structures using semiautomatic segmentation. Yellow, axonemal MTs; red, IFT trains; white, flagellar membrane; green, glycocalyx. (c and d) These sectioning levels show the links of IFT trains with the flagellar membrane and reveal a structural pattern very similar to that shown in Fig. 6, panel 1. (e and f) In *fla14* flagella, IFT trains are frequently visible on top of each other, giving rise to multiple layers of IFT trains (arrows). All the images are oriented so that the tip of flagellum points to the left of the plate. Video 1 shows a tomographic reconstruction related to panel a.

compact than that of the long trains, which are less opaque and more spread out. Consequently, the short trains are less suitable for the averaging protocols used for modeling the long IFT trains. The short, compact, and more opaque retrograde trains, like the long trains, also vary in structure depending on the level of longitudinal sectioning.

By sectioning at three different levels along the z axis of the tomograms of IFT retrograde trains, we observed the patterns shown in Fig. 9. Fig. 9 (a and d) shows the association of IFT trains with the flagellar membrane. At this sectioning level, IFT trains also show projections linking them to the MT doublets. Fig. 9 (b and e), sectioned at the level of the axial core of the retrograde IFT trains, reveals the presence of a rodlike

structure at the interface between the MT doublet and the rest of IFT train facing the flagellar membrane. This structure appears to be continuous, running along the length of the IFT train and parallel to the longitudinal axis of the MT doublet, with no obvious internal periodicity. Fig. 9 (c and f) shows sections of the retrograde IFT trains cut through the “lollipop-shaped” particles previously described by others in short, dense IFT trains (Kozminski et al., 1993, 1995; Dentler, 2005; Pedersen et al., 2006) in *C. reinhardtii* flagella. These “lollipop-like” particles occur along the IFT trains with a 16-nm repeat, as previously observed in 2D EM pictures of short trains (Fig. 2 e). Colored diagrams superimposed onto the original pictures are shown in Fig. 9 (g, h, and i) to highlight these ultrastructural features.

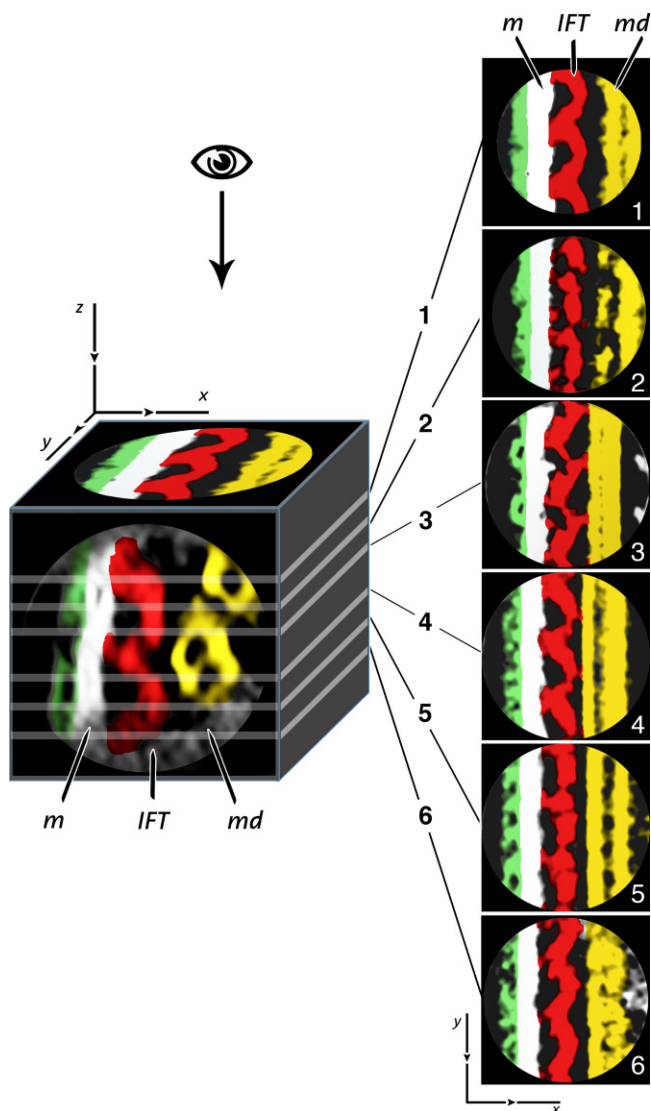


Figure 6. Sectioning of the 3D density map obtained by aligning and averaging IFT particles from *fla14* mutant cells. The density map was obtained by averaging 15 tomographic volumes from a single train, each one containing three contiguous IFT particles as shown in the inset of Fig. 5 a. The images 1–6 were produced by serial sectioning along the z axis of the cubic volume shown on the left. To illustrate the spatial orientation of sectioning planes in the model, a cross section of it is shown on the frontal face of the cube and a longitudinal section is shown on the top face. The cutting planes, represented by the white lines on the cube, are numbered from 1 to 6, proceeding along the z axis from the top to the bottom of the 3D map. Each section is 0.66 nm thick. The glycocalyx, the flagellar membrane (m), the IFT, and the MT doublet (md) have been manually segmented using the same color coding shown in Fig. 5 (green, glycocalyx; white, membrane; red, IFT particles; yellow, MT doublet). This kind of rendering revealed fine structural details of IFT particles with patterning variations depending on the sectioning level of the 3D density map. Panels are oriented so that the tip of flagellum is oriented downward.

One of the tomograms obtained by dual-axis tomography of a retrograde IFT train from WT flagella was processed by semiautomatic segmentation. The longitudinal view in Fig. 10 a shows the retrograde IFT train in the space between the plasma membrane and the MT doublet. Its left end (the one pointing toward the cell body) is slender and thinner than its opposite end, which displays a more rounded contour. This asymmetry

between the two ends of the IFT train is confirmed when the surface model of this same IFT train is observed from the inside of the axoneme looking out toward the membrane (Fig. 10 b) and from the outside of the flagellum, looking inward the MT doublet, with the membrane removed (Fig. 10 c); this suggests the presence of a polarity in the retrograde train. The IFT train in Fig. 10 measures ~ 250 nm \times 50 nm \times 20 nm. For a direct comparison between surface renderings of long and short trains, see Fig. S4.

Discussion

Although IFT was described over 15 yr ago (Kozminski et al., 1993), the ultrastructural basis for IFT has received little attention. In the initial description of IFT, linear arrays of electron-opaque particles were identified by TEM lying between the flagellar membrane and the outer doublet MTs, and were hypothesized to be the structures being moved by IFT (Kozminski et al., 1993). This relationship was confirmed soon thereafter using correlative DIC microscopy and EM of flat-embedded cells showing that the varicosities seen moving along the flagella by DIC microscopy (Kozminski et al., 1993) corresponded to the electron-dense rows or trains of IFT particles between the membrane and the outer doublet MTs (Kozminski et al., 1995). These early electron micrographs showed hints of periodicities of “lollipop-shaped” subunits that composed the IFT trains as well as links between the B tubules of the outer MT doublets and the trains (Kozminski et al., 1993).

Even these initial observations of IFT suggested that anterograde and retrograde IFT trains were different: anterograde IFT movement was easier to visualize by DIC imaging than retrograde movement (Kozminski et al., 1993) because the varicosities appeared larger than the retrograde varicosities. The size difference visualized by DIC microscopy was reflected in kymographs of IFT in which the traces of anterograde varicosities were wider than those of retrograde varicosities (Piperno et al., 1998; Iomini et al., 2001), but these images provided little information about the size or structure of the IFT train underlying the membrane. Despite the different size of anterograde and retrograde varicosities seen by DIC, the typical IFT train shown by EM in the literature was ~ 250 nm long, with distinct anterior and posterior ends. Certainly, this was what Ringo (1967) described in his early study of these structures. We now recognize that WT flagella also contain a second class of IFT trains that are more heterogeneous in length, less electron opaque, and that have anterior and posterior boundaries that are less well defined. In individual planes of tomographic reconstructions, the appearance of the two categories of trains is also different: the shorter and more compact IFT trains show a repeat of 16 nm, whereas the longer trains have a repeat of ~ 40 nm. Furthermore, the long IFT trains are more amenable to tomographic analysis than short trains because of their relatively open structure. Such analysis suggests that each unit of the long anterograde train is made of two similar particles, so the train appears to be made up of a double string of particles.

The tomograms and the 3D models of long IFT trains presented in this paper were derived from flagella of the retrograde

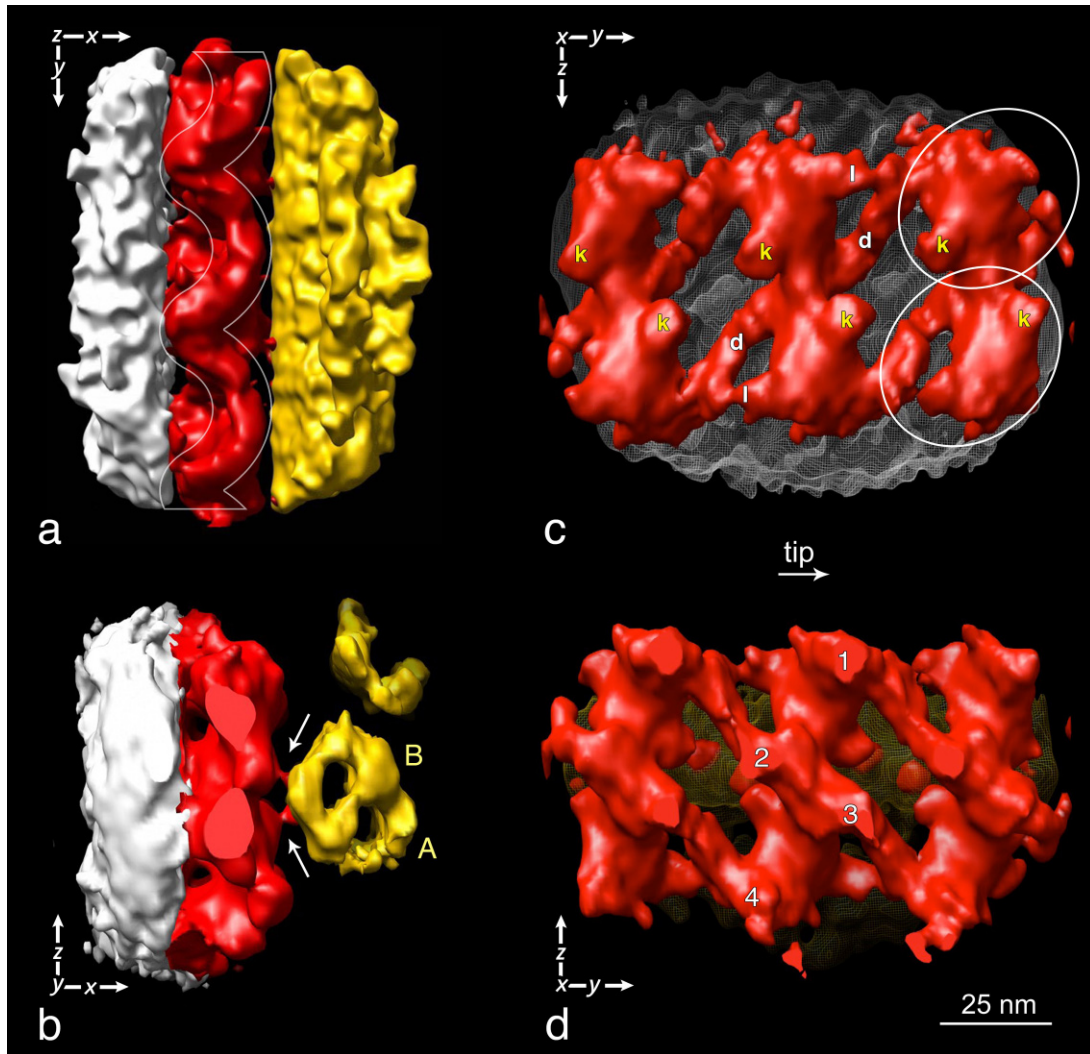


Figure 7. Four different views of a surface-rendering representation of the 3D model of IFT particles in *fla14* flagella. Colors have been assigned to sub-volumes of the density map corresponding to different flagellar structures using the same color coding shown in Figs. 5 and 6 (white, flagellar membrane; red, IFT particles; yellow, MT doublets). In this and subsequent figures, the images are oriented so that the flagella point down or to the right. (a) The white lines highlight the festooned profile of the IFT particles. The same wave pattern is seen in Fig. 6, panel 1, and Fig. 2 (f–o). (b) Cross-section view of the same model oriented so that the tip of flagellum points toward the reader. The white arrows indicate the position of the links between each IFT particle and the B subtubule of the MT doublet (B). A, A subtubule of the MT doublet. (c) Three pairs of IFT particles lying on the flagellar membrane (white wire net pattern) as seen from the interior of the axoneme. Oblique links (d) connect neighboring particles (white ovals) along each strand. Links (l), oriented parallel to the longitudinal axis of IFT trains, connect the heads of adjacent particles. The position of the links between IFT particles and the B subtubule of the MT doublet are labeled with a k, and may be the kinesin-2 motors. (d) The pairs of IFT particles as seen from the exterior of the flagellum. The yellow net behind them represents the outer surface of an MT doublet. 1, 2, 3, and 4 indicate the contact points between IFT particles and the flagellar membrane. Video 2 shows a rotation of the surface-rendered model.

mutant *fla14* cells because of the abundance of IFT trains in these flagella. Unlike other retrograde mutants (Piperno et al., 1998), *fla14* does not present any deficiency in IFT proteins of either complex A or complex B (Pazour et al., 1998). These *fla14* IFT trains, therefore, appear to be assembled normally, with the same structure as the long trains in WT cells. This was confirmed by comparing longitudinal sections of long IFT trains from WT and *fla14* (Figs. 2 and S2) and by comparing sections of the 3D model, which was based on data derived from *fla14* (Figs. 6 and 7), to sections of WT trains shown in Fig. 2. Only the long category of IFT train was found in *fla14*, and this retrograde IFT mutant displays anterograde but not retrograde IFT (Pazour et al., 1998), which strongly suggests that the longer,

less opaque trains are anterograde trains and the shorter, compact trains are retrograde trains.

Another explanation for the existence of short and long trains, however, is that both categories of trains are traveling in both directions, and that the short trains represent long trains that have picked up cargo either at the flagellar base or tip. The long trains would, therefore, represent empty IFT trains. According to this hypothesis, *fla14* has principally long, thin trains because it lacks much of the cargo present in WT flagella; e.g., dynein arms and radial spokes. The reduction of cargo would result in a predominance of long (unloaded) trains. We are currently testing this possibility by quantifying the number of long and short trains in flagella of

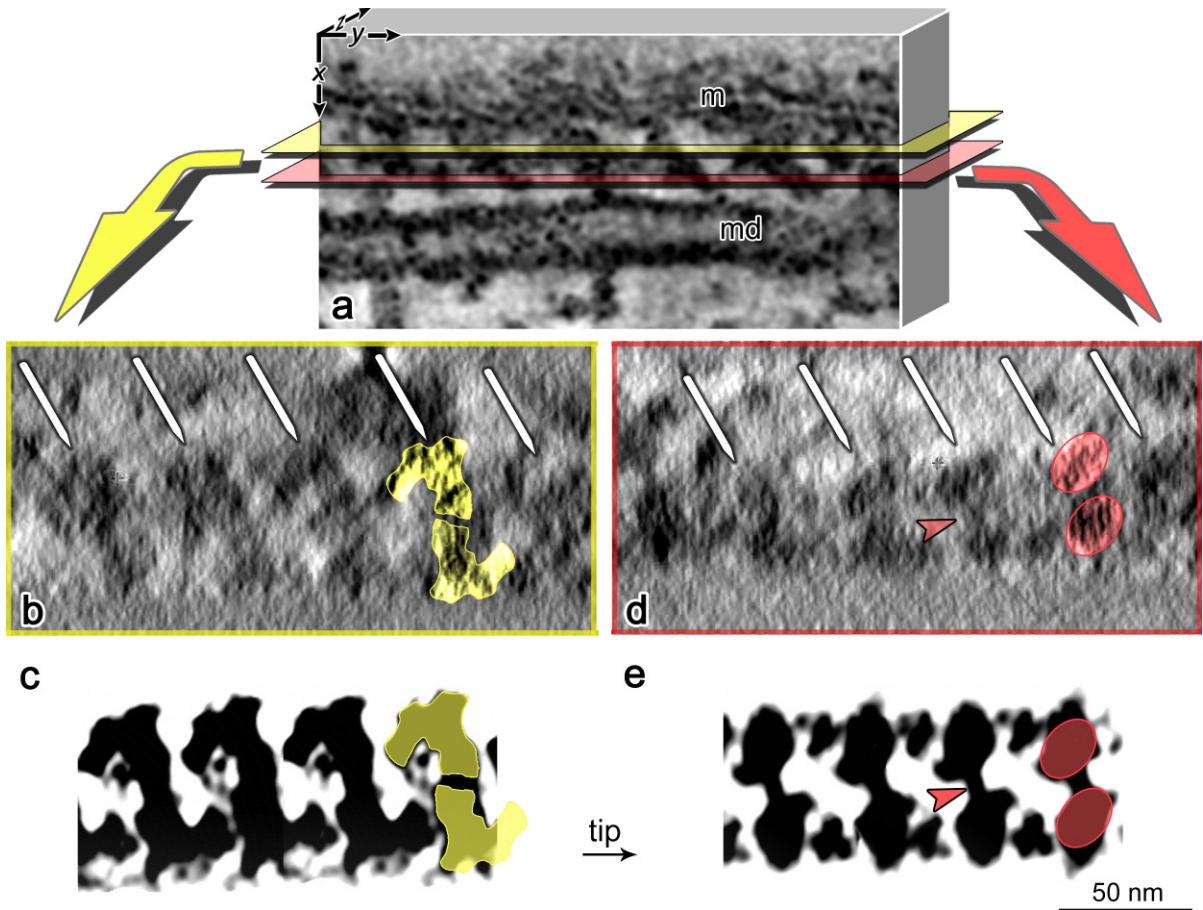


Figure 8. Comparison of sections of IFT trains from a tomogram and the 3D model. (a) Schematic representation of part of a tomogram from a *fla14* flagellum. The selected volume contains part of an IFT train, located in the space between the flagellar membrane (m) and an MT doublet (md). (b and d) Virtual sections (~15 nm thick) obtained by sectioning the reconstructed volume tangentially to the axoneme, between the flagellar membrane and the MT doublet (as shown in panel a), thus sectioning the IFT train longitudinally. The white arrows indicate the IFT particles aligned along the train. (c and e) Individual planes of IFT particles from *fla14* flagella maps after tomographic reconstruction and particle averaging. The planes are cut with the same orientation and at levels comparable to those in panels b and d. Notice the strong similarity of IFT sectioning contours between panels b and c and panels d and e. Colored masks are used to highlight the similarity of the structures in panels b and c (yellow masks) and d and e (red masks), and the similarity between the particles composing each IFT unit. The arrowheads in panels d and e indicate the link between the top and the bottom IFT particles.

cells that are known to have either more, or less, cargo associated with the IFT trains.

The 3D model shows links connecting adjacent subunits together to form the long IFT trains (Fig. 7). Because the IFT trains are easily disrupted to yield soluble A and B complexes (Cole et al., 1998), which move separately in sucrose gradients, it has been suggested that adjacent IFT particles have relatively weak interactions with each other (Lucker et al., 2005). Despite the predicted weakness of such links, they are visible in the tomograms and are enhanced by the averaging protocol used to generate the 3D model (Fig. 7 c). The model shows that links are located in constant positions in every particle contributing to the average, and are, therefore, rigid structures. Perhaps the strongest evidence for self-sustaining links between the IFT units, and between their constitutive particles, is the *in situ* observation in this study that chains of IFT units can be observed in the bulges of *fla14* flagella, under conditions where they are not in association with either the flagellar membrane or the axoneme (Fig. 5 b, white ovals).

The 3D model of IFT units from anterograde trains also shows bridges between the particles and the B subtube of MT

doublets (Fig. 7 b, arrows; and Fig. 7 c, “k”). These connections may represent the position of the anterograde motor, kinesin-2. If there is one kinesin in every 40 nm, our model predicts a ratio of one putative kinesin for every five tubulin dimers (8 nm/dimer) along an outer doublet protofilament. The presence of these links is also supported by the analysis of cross ultrathin sections of *C. reinhardtii* flagella, where pairs of IFT particles are often linked to the B subtube by two electron-dense bridges (Figs. 1 b and 4). Although these bridges are located between the IFT particles and the MTs, where one would expect to find kinesin motors, as of yet we have no direct evidence of the molecular nature of the bridges.

At present, we know very little about the molecular composition of the various protrusions/extensions/connections from the IFT particles observed in the tomograms, or even about the placement of motors or complex A and B in the IFT trains. This could be determined by analysis of various IFT mutants lacking certain IFT polypeptides using electron tomographic techniques similar to those used in this paper, as well as cryo-EM of isolated IFT particles. Indeed, *C. reinhardtii* IFT mutant *fla15*

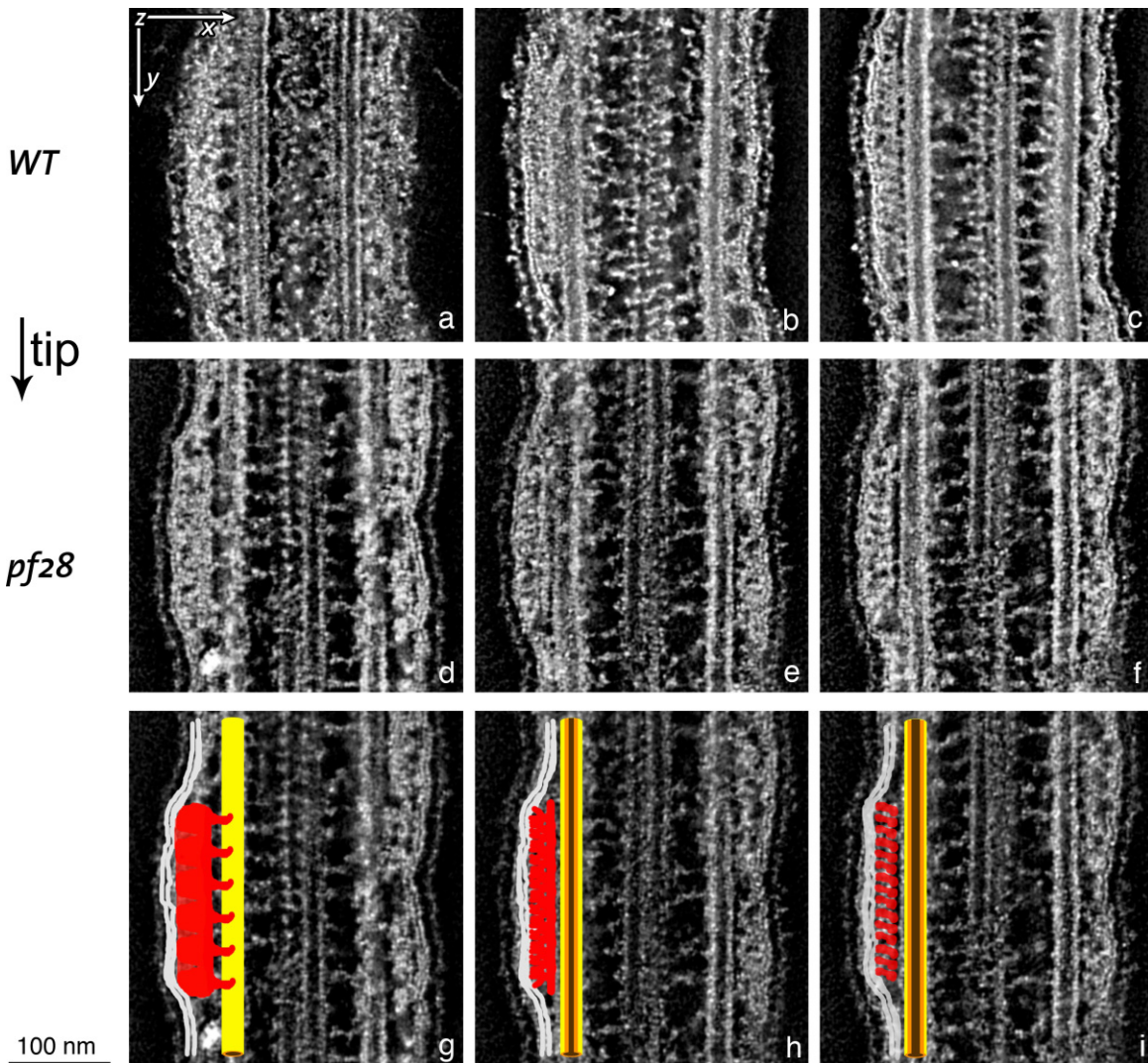


Figure 9. Serial sectioning of tomograms obtained from flat-embedded flagella of WT and *pf28* mutant *C. reinhardtii* cells showing short IFT trains. The ~5-nm-thick virtual sections are cut along the longitudinal axis of the axoneme. The three selected cutting planes show ultrastructural features of the short IFT trains that are routinely observed in tomograms obtained from both WT and *pf28* flagella. (a–c) Sections of a short train from a WT flagellum. (d–f) Sections of a short train from a *pf28* flagellum. Panels a and d show the association of IFT trains with the flagellar membrane. Projections linking the IFT trains to the MT doublet, possibly cytoplasmic dynein 1b because these are retrograde IFT trains, are also visible at this sectioning level. Sections b and e are cut through the axial core of the IFT train, and show the presence of a rodlike structure running parallel to the longitudinal axis of the MT doublet with no internal periodicity. Panels c and f show sections of IFT trains cut through the lollipop-like particles visible along the IFT trains with a 16-nm repeat. (g–i) Colored diagrams superimposed onto panels d–f to highlight the ultrastructural features shown in a–f. White, flagellar membrane; red, IFT train; yellow/brown, MT doublet.

lacks almost all of its complex A polypeptides (Piperno et al., 1998), and its analysis by electron tomography and cryo-EM should provide valuable insight into the localization of complex A polypeptides within the IFT train. Likewise, the retrograde trains in the mutant *fla24* appear by DIC microscopy to be as large as the anterograde IFT varicosities in WT (Iomini et al., 2001); this mutant, too, may provide important information on IFT train structure. We have been able to isolate flagellar membranes with attached IFT trains (Huang et al., 2007; Mencarelli, C., and A. Mitchell, personal communication), and this should provide material for cryo-EM studies of isolated IFT trains from flagella of WT and mutant cells.

We also do not know where the IFT cargo is located, and analysis of cross and longitudinal sections provides little

information on its placement. Cargo could be associated with the IFT trains themselves, and/or it could be associated with the inner aspect of the flagellar membrane, being moved by the underlying IFT trains, which appear to be tightly associated with the inner surface of the flagellar membrane (Fig. S3). This latter possibility is appealing, not only because of the ultrastructural evidence for IFT–membrane associations, but because it has been proposed (Rosenbaum and Witman, 2002) that some IFT cargo, synthesized on free polysomes (e.g., tubulin) might become associated with the outer surface of cytoplasmic vesicles before their exocytosis near the basal body. Once these vesicles progressed through exocytosis, the cargo proteins would be associated with the inner aspect of the flagellar membrane, as well as with the IFT trains, which, like cargo, become associated

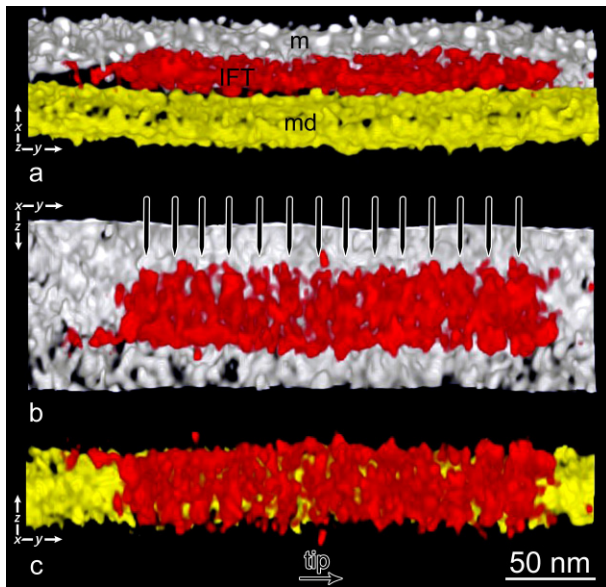


Figure 10. Surface rendering of a short retrograde IFT train from a WT flagellum tomogram. The density map was semiautomatically segmented, and colors have been assigned as in previous models (white, flagellar membrane [m]; red, IFT particles [IFT]; yellow, MT doublets [md]). (a) Longitudinal view of the model. The IFT train is located in the space between the flagellar membrane and the MT doublet. The two ends of the IFT train have different appearances, which suggests the presence of a polarity in the retrograde train. (b) The retrograde IFT train as seen from the interior of the axoneme. (c) The IFT train as seen from the exterior of the axoneme. Note in b and c the asymmetry between the head and the tail ends, and the presence of repeating structures along the train. Black arrows in each frame indicate the flagellar tip orientation.

with the vesicles before exocytosis (Rosenbaum and Witman, 2002; Follit et al., 2006). This hypothesis is currently being tested by isolating cytoplasmic vesicles, and determining what flagellar proteins, both membrane and axonemal, are present on the vesicles as well as on isolated flagellar membranes.

Evidence for an interaction of IFT and cytoplasmic vesicles comes from work on IFT20, a peripheral subunit of the complex B (Lucker et al., 2005) that may play a role in trafficking of ciliary membrane proteins from the Golgi complex into the cilium (Follit et al., 2006). The fact that IFT20 is involved in movement of vesicles from the Golgi to the ciliary membrane may implicate complex B as being associated with these vesicles near the base of the flagella and subsequently on the inner aspect of the flagellar membrane (Follit et al., 2006). A functional association of IFT trains with proteins in the flagellar membrane is known to occur, as best illustrated by the movement of transient receptor potential vanilloid membrane channels in *Caenorhabditis elegans* cilia at the rates of IFT, which suggests that IFT transports proteins within and along the ciliary membrane (Qin et al., 2005). Likewise, in *C. reinhardtii*, movement of PKD-2 (polycystin-2), another multipass membrane channel, is dependent on IFT (Huang et al., 2007). Thus, both structural and functional data support an interaction of IFT trains with the flagellar membrane.

Currently, there is clear evidence for the requirement of IFT46 in the transport of outer arm dynein, from the cytoplasm to the flagellar tip assembly site (Hou et al., 2007). There is also

strong evidence for the association of axonemal radial spoke precursors with the IFT particles during their transport to the tip assembly site (Qin et al., 2004). It is not known, however, if these precursors are also associated with cytoplasmic vesicles and with the flagellar membrane during their transport to the flagellar tip. Antibody labeling of cytoplasmic vesicles and of flagella cross and longitudinal sections from WT and mutant cells should provide information on cargo localization.

Although the 3D model for IFT trains presented here provides new insights concerning the ultrastructure of anterograde IFT trains, less was learned about the retrograde trains because their intrinsic morphology is more problematic for image averaging protocols. In unaveraged tomograms, retrograde IFT trains are complex, compact, electron-opaque structures characterized by a highly variable structure and different patterns and repeats along different sectioning planes of the 3D model. In spite of the lack of detail obtained on the ultrastructure of the retrograde IFT trains, the data in this paper provide a 3D view of anterograde IFT trains and a dramatic representation of the extensive restructuring that must accompany the conversion of anterograde to retrograde IFT trains at the flagellar tip.

Materials and methods

Sample preparation: flat-embedding

C. reinhardtii cells were pipetted onto clean glass coverslips (18 × 18 mm, # 1; Carl Roth GmbH) and allowed to settle and adhere for 5–15 min (Mitchell and Nakatsugawa, 2004; Pedersen et al., 2006). The coverslips were gently washed by immersion into MI culture medium, and the cells were fixed by pipetting MI containing 2.5% glutaraldehyde (Serva Electrophoresis), pH 7.2, onto the coverslips. After 30 min at RT, the fixative was replaced with MI containing 2.5% glutaraldehyde and 0.2–0.4% tannic acid (Mallinckrodt Baker), pH 7.2, and the fixation continued for another 30 min at RT. After a rinse with distilled water, the cells were postfixed with 1% OsO₄ (in distilled water) at 4°C for 30 min. After washes with distilled water, the specimens were dehydrated using a graduated series of ethanol and infiltrated with epon 812 (Serva Electrophoresis). Polymerization was performed for 48 h at 65°C and the coverslips were dissolved off the epon layer by immersion in hydrofluoric acid. Areas of interest were cut out of the flat embeddings under a dissecting microscope and mounted on dummy blocks using two-component epoxy adhesive (UHU plus endfest 300; UHU GmbH and Co. KG). When cutting longitudinal sections of the flagella, a very accurate alignment of the block face with the diamond knife is essential, as flagella are ~250-nm thick and only the first few sections contain flagella. Serial sections (~60 nm for standard TEM and 100 nm for tomography) were cut with a diamond knife (type ultra 35°; Diatome) on an ultramicrotome (EM UC6; Leica) and collected on formvar-coated 100 hexagonal mesh copper-rhodium grids. Specimens were stained with lead citrate and uranyl acetate (Reynolds, 1963).

TEM and electron tomography

Standard TEM was done using a transmission electron microscope (JEM-2100; JEOL Ltd.) equipped with a 4,000 × 4,000 charge-coupled device camera (UltraScan 4000; Gatan, Inc.) and Gatan Digital Micrograph software (version 1.70.16.). Tomography was performed with a transmission electron microscope CM200 field emission gun (Philips) operating at 160 kv, equipped with a 2,000 × 2,000 charge-coupled device camera (TVIPS TemCam-F224HD) and the EMmenu4 software package (both from Tietz Video and Image Processing Systems GmbH). 100-nm-thick sections were decorated on both faces with 10 nm colloidal gold particles before observation in the Philips transmission electron microscope. Gold particles were used as position fiducial markers for image alignment in the tomogram reconstruction procedure. For tomographic reconstruction, low-dose tilt series of images were recorded in double tilt axis geometry, at 27,500× magnification (nominal pixel size 0.66 nm), with a maximum tilt range of about 60° and tilt steps of 1°, with a cumulative electron dose below 17,000 e⁻/nm². Images were recorded with 1 μm of defocus.

Image analysis

3D reconstruction was performed using R-weighted back-projection with IMOD software (Kremer et al., 1996; Mastronarde, 1997) and other packages developed in Milano; in the latter case, we exported the 2D coordinates of the fiducial markers acquired with IMOD and pasted the two series of reference points together with simultaneous alignment. The reconstruction was then performed using a weighted back-projection algorithm for general geometry (Radermacher, 1992) and local refinement for distortions correction (Cantele et al., 2007).

The shrinkage of the volume varied slightly from map to map, depending on the number of exposures; we calibrated the final pixel size of tomograms on the basis of the periodicities of the axoneme. The resolution of the volume was then measured using even/odd Fourier Shell Correlation between independent copies of the tomogram, as described by Cardone et al. (2005), and was determined to be $\sim 4\text{--}5$ nm, using the 0.5 criterion.

The trains of IFT particles contained multiple copies of the same complexes arranged in rows. The size of the particles was measured by counting how many of them were aligned along trains of known length. We then applied the "3D particle averaging strategy" (Walz et al., 1997; Nicastro et al., 2005; Ishikawa et al., 2007; Bui et al., 2008) to enhance their signal/noise ratio. Volumes (200 pixel cube) including three repeats of IFT particles, together with MT doublets, were excised out of the tomogram using Bshow program (Heymann, 2001). IFT particles from each extracted volume were aligned and averaged with Spider (Frank et al., 1996) by a reference-based alignment strategy. A single representative volume, containing three particles, from the set of volumes identified in the first step was used as a reference. To avoid bias in the resulting estimation, multiple randomly chosen references were used. Multiple search iterations were applied and a refined reference, estimated from the average of the aligned particles, was used in the successive alignment steps. Because particles from only one IFT train were included in each average, compensation for the missing wedge was unnecessary because all particles possessed almost the same orientation with respect to the tilting axis.

Both the reconstructed tomograms and averaged maps were semi-automatically segmented by use of the software JUST (Java User Segmentation Tool; Salvi et al., 2008). Segmented structures were visualized with Chimera (Petersen et al., 2004) or Avizo (Mercury Computer Systems, Inc.) by surface- or by volume-rendering techniques.

Nomenclature

When the first electron micrographs of IFT structure *in situ* were published (Kozminski et al., 1993, 1995), the rows of particles between the membrane and axoneme were called "rafts." This term was confusing because of its use to describe membrane lipid arrays. The rows of IFT particles are now called IFT "trains." The use of the term train is appropriate because the particles are carrying both flagellar membrane and axonemal cargoes (Rosenbaum and Witman, 2002; Qin et al., 2004, 2005; Ou et al., 2005; Bae et al., 2006; Hou et al., 2007). The long trains are composed of two rows of individual IFT particles.

Online supplemental material

Fig. S1 shows the analysis of the number of IFT trains per flagellum using serial section TEM. Fig. S2 shows longitudinal, virtual sections through a tomogram of a WT and a *fla14* flagellum. Fig. S3 shows a schematic cross section of a *C. reinhardtii* flagellum showing the organization of an antero-grade IFT train. Fig. S4 shows a combination of Figs. 7 and 10 for direct comparison between 3D surface-rendering models of long and short IFT trains. Video 1 shows a "virtual flight" along the z axis of a tomographic reconstruction obtained from a flagellum of the *fla14* *C. reinhardtii* mutant. Video 2 shows rotation of surface-rendering model of three anterograde IFT units from a *fla14* mutant cell. Table S1 shows the number of IFT trains per flagellum as determined by serial section standard EM.

We wish to thank Elisa Vannuccini (University of Siena) and Dirk Scholz (University of Bayreuth) for technical assistance and Caterina Mencarelli (University of Siena) and Romano Dallai (University of Siena) for stimulating discussions during the course of this work. We thank Christopher R. Wood (Yale University) for the hypothesis that the short IFT trains carry cargo in both directions.

These studies were supported by grants from Telethon (GGP07269) and Monte dei Paschi di Siena (2008-2009) to P. Lupetti and the National Institutes for Health (NIH-GMS-14642) to J.L. Rosenbaum.

Submitted: 19 May 2009

Accepted: 3 September 2009

References

- Bae, Y.-K., H. Qin, K.M. Knobel, J. Hu, J.L. Rosenbaum, and M.M. Barr. 2006. General and cell-type specific mechanisms target TRPP2/PKD-2 to cilia. *Development*. 133:3859–3870. doi:10.1242/dev.02555
- Beech, P.L., K. Pagh-Roehl, Y. Noda, N. Hirokawa, B. Burnside, and J.L. Rosenbaum. 1996. Localization of kinesin superfamily proteins to the connecting cilium of fish photoreceptors. *J. Cell Sci.* 109:889–897.
- Bloodgood, R.A. 1981. Flagella-dependent gliding motility in *Chlamydomonas*. *Protoplasma*. 106:183–192. doi:10.1007/BF01275550
- Bui, K.H., H. Sakakibara, T. Movassagh, K. Oiwa, and T. Ishikawa. 2008. Molecular architecture of inner dynein arms *in situ* in *Chlamydomonas reinhardtii* flagella. *J. Cell Biol.* 183:923–932. doi:10.1083/jcb.200808050
- Cantele, F., L. Zampighi, M. Radermacher, G. Zampighi, and S. Lanzavecchia. 2007. Local refinement: an attempt to correct for shrinkage and distortion in electron tomography. *J. Struct. Biol.* 158:59–70. doi:10.1016/j.jsb.2006.10.015
- Cardone, G., K. Grünewald, and A.C. Steven. 2005. A resolution criterion for electron tomography based on cross-validation. *J. Struct. Biol.* 151:117–129. doi:10.1016/j.jsb.2005.04.006
- Cole, D.G., D.R. Diener, A.L. Himelblau, P.L. Beech, J.C. Fuster, and J.L. Rosenbaum. 1998. *Chlamydomonas* kinesin-II-dependent intraflagellar transport (IFT): IFT particles contain proteins required for ciliary assembly in *Caenorhabditis elegans* sensory neurons. *J. Cell Biol.* 141:993–1008. doi:10.1083/jcb.141.4.993
- Dentler, W. 2005. Intraflagellar transport (IFT) during assembly and disassembly of *Chlamydomonas* flagella. *J. Cell Biol.* 170:649–659. doi:10.1083/jcb.200412021
- Follit, J.A., R.A. Tuft, K.E. Fogarty, and G.J. Pazour. 2006. The intraflagellar transport protein IFT20 is associated with the Golgi complex and is required for cilia assembly. *Mol. Biol. Cell.* 17:3781–3792. doi:10.1091/mbc.E06-02-0133
- Frank, J., M. Radermacher, P. Penczek, J. Zhu, Y. Li, M. Ladadji, and A. Leith. 1996. SPIDER and WEB: processing and visualization of images in 3D electron microscopy and related fields. *J. Struct. Biol.* 116:190–199. doi:10.1006/jsb.1996.0030
- Heymann, J.B. 2001. Bsoft: image and molecular processing in electron microscopy. *J. Struct. Biol.* 133:156–169. doi:10.1006/jsb.2001.4339
- Hou, Y., H. Qin, J.A. Follit, G.J. Pazour, J.L. Rosenbaum, and G.B. Witman. 2007. Functional analysis of an individual IFT protein IFT46 is required for transport of outer dynein arms into flagella. *J. Cell Biol.* 176:653–665. doi:10.1083/jcb.200608041
- Huang, K., D.R. Diener, A. Mitchell, G.J. Pazour, G.B. Witman, and J.L. Rosenbaum. 2007. Function and dynamics of PKD2 in *Chlamydomonas reinhardtii* flagella. *J. Cell Biol.* 179:501–514. doi:10.1083/jcb.200704069
- Iomini, C., V. Babaev-Khaimov, M. Sassaroli, and G. Piperno. 2001. Protein particles in *Chlamydomonas* flagella undergo a transport cycle consisting of four phases. *J. Cell Biol.* 153:13–24. doi:10.1083/jcb.153.1.13
- Ishikawa, T., H. Sakakibara, and K. Oiwa. 2007. The architecture of outer dynein arms *in situ*. *J. Mol. Biol.* 368:1249–1258. doi:10.1016/j.jmb.2007.02.072
- King, S.M., E. Barbarese, J.F. Dillman III, R.S. Patel-King, J.H. Carson, and K.K. Pfister. 1996. Brain cytoplasmic and flagellar outer arm dyneins share a highly conserved $M_8,000$ light chain. *J. Biol. Chem.* 271:19358–19366. doi:10.1074/jbc.271.32.19358
- Kozminski, K.G., K.A. Johnson, P. Forscher, and J.L. Rosenbaum. 1993. A motility in the eukaryotic flagellum unrelated to flagellar beating. *Proc. Natl. Acad. Sci. USA*. 90:5519–5523. doi:10.1073/pnas.90.12.5519
- Kozminski, K.G., P.L. Beech, and J.L. Rosenbaum. 1995. The *Chlamydomonas* kinesin-like protein FLA10 is involved in motility associated with the flagellar membrane. *J. Cell Biol.* 131:1517–1527. doi:10.1083/jcb.131.6.1517
- Kremer, J.R., D.N. Mastronarde, and J.R. McIntosh. 1996. Computer visualization of three-dimensional image data using IMOD. *J. Struct. Biol.* 116:71–76. doi:10.1006/jsb.1996.0013
- Lucker, B.F., R.H. Behal, H. Qin, L.C. Siron, W.D. Taggart, J.L. Rosenbaum, and D.G. Cole. 2005. Characterization of the intraflagellar transport complex B core: direct interaction of the IFT81 and IFT74/72 subunits. *J. Biol. Chem.* 280:27688–27696. doi:10.1074/jbc.M505062200
- Marshall, W.F., and J.L. Rosenbaum. 2001. Intraflagellar transport balances continuous turnover of outer doublet microtubules: implications for flagellar length control. *J. Cell Biol.* 155:405–414. doi:10.1083/jcb.200106141
- Mastronarde, D.N. 1997. Dual-axis tomography: an approach with alignment methods that preserve resolution. *J. Struct. Biol.* 120:343–352. doi:10.1006/jsb.1997.3919
- Mitchell, D.R., and M. Nakatsugawa. 2004. Bend propagation drives central pair rotation in *Chlamydomonas reinhardtii* flagella. *J. Cell Biol.* 166:709–715. doi:10.1083/jcb.200406148

- Nicastro, D., J.R. McIntosh, and W. Baumeister. 2005. 3D structure of eukaryotic flagella in a quiescent state revealed by cryo-electron tomography. *Proc. Natl. Acad. Sci. USA.* 102:15889–15894. doi:10.1073/pnas.0508274102
- Orozco, J.T., K.P. Wedaman, D. Signor, H. Brown, L. Rose, and J.M. Scholey. 1999. Movement of motor and cargo along cilia. *Nature.* 398:674. doi:10.1038/19448
- Ou, G., H. Qin, J.L. Rosenbaum, and J.M. Scholey. 2005. The PKD protein qilin undergoes intraflagellar transport. *Curr. Biol.* 15:R410–R411. doi:10.1016/j.cub.2005.05.044
- Pazour, G.J., C.G. Wilkerson, and G.B. Witman. 1998. A dynein light chain is essential for the retrograde particle movement of intraflagellar transport (IFT). *J. Cell Biol.* 141:979–992. doi:10.1083/jcb.141.4.979
- Pazour, G.J., B.L. Dickert, and G.B. Witman. 1999. The DHC1b (DHC2) isoform of cytoplasmic dynein is required for flagellar assembly. *J. Cell Biol.* 144:473–481. doi:10.1083/jcb.144.3.473
- Pazour, G.J., B.L. Dickert, Y. Vucica, E.S. Seeley, J.L. Rosenbaum, G.B. Witman, and D.G. Cole. 2000. *Chlamydomonas* IFT88 and its mouse homologue, polycystic kidney disease gene tg737, are required for assembly of cilia and flagella. *J. Cell Biol.* 151:709–718. doi:10.1083/jcb.151.3.709
- Pazour, G.J., S.A. Baker, J.A. Deane, D.G. Cole, B.L. Dickert, J.L. Rosenbaum, G.B. Witman, and J.C. Besharse. 2002. The intraflagellar transport protein, IFT88, is essential for vertebrate photoreceptor assembly and maintenance. *J. Cell Biol.* 157:103–113. doi:10.1083/jcb.200107108
- Pedersen, L.B., and J.L. Rosenbaum. 2008. Intraflagellar transport (IFT) role in ciliary assembly, resorption and signalling. *Curr. Top. Dev. Biol.* 85:23–61. doi:10.1016/S0070-2153(08)00802-8
- Pedersen, L.B., S. Geimer, and J.L. Rosenbaum. 2006. Dissecting the molecular mechanisms of intraflagellar transport in *Chlamydomonas*. *Curr. Biol.* 16:450–459. doi:10.1016/j.cub.2006.02.020
- Pettersen, E.F., T.D. Goddard, C.C. Huang, G.S. Couch, D.M. Greenblatt, E.C. Meng, and T.E. Ferrin. 2004. UCSF Chimera—a visualization system for exploratory research and analysis. *J. Comput. Chem.* 25:1605–1612. doi:10.1002/jcc.20084
- Piperno, G., and D.J.L. Luck. 1979. Axonemal adenosine triphosphatases from flagella of *Chlamydomonas reinhardtii*. Purification of two dyneins. *J. Biol. Chem.* 254:3084–3090.
- Piperno, G., E. Siuda, S. Henderson, M. Segil, H. Vaananen, and M. Sassaroli. 1998. Distinct mutants of retrograde intraflagellar transport (IFT) share similar morphological and molecular defects. *J. Cell Biol.* 143:1591–1601. doi:10.1083/jcb.143.6.1591
- Qin, H., D.R. Diener, S. Geimer, D.G. Cole, and J.L. Rosenbaum. 2004. Intraflagellar transport (IFT) cargo: IFT transports flagellar precursors to the tip and turnover products to the cell body. *J. Cell Biol.* 164:255–266. doi:10.1083/jcb.200308132
- Qin, H., D.T. Burnette, Y.K. Bae, P. Forscher, M.M. Barr, and J.L. Rosenbaum. 2005. Intraflagellar transport is required for the vectorial movement of TRPV channels in the ciliary membrane. *Curr. Biol.* 15:1695–1699. doi:10.1016/j.cub.2005.08.047
- Radermacher, M. 1992. Weighted backprojection methods. In *Electron Tomography*. J. Frank, editor. Plenum Press, New York. 91–116.
- Reynolds, E.S. 1963. The use of lead citrate at high pH as an electron-opaque stain in electron microscopy. *J. Cell Biol.* 17:208–212. doi:10.1083/jcb.17.1.208
- Ringo, D.L. 1967. Flagellar motion and fine structure of the flagellar apparatus in *Chlamydomonas*. *J. Cell Biol.* 33:543–571. doi:10.1083/jcb.33.3.543
- Rosenbaum, J.L., and G.B. Witman. 2002. Intraflagellar transport. *Nat. Rev. Mol. Cell Biol.* 3:813–825. doi:10.1038/nrm952
- Rosenbaum, J.L., D.G. Cole, and D.R. Diener. 1999. Intraflagellar transport: the eyes have it. *J. Cell Biol.* 144:385–388. doi:10.1083/jcb.144.3.385
- Salvi, E., F. Cantele, L. Zampighi, N. Fain, G. Pigino, G. Zampighi, and S. Lanzavecchia. 2008. JUST (Java User Segmentation Tool) for semi-automatic segmentation of tomographic maps. *J. Struct. Biol.* 161:287–297. doi:10.1016/j.jsb.2007.06.011
- Scholey, J.M. 2003. Intraflagellar transport. *Annu. Rev. Cell Dev. Biol.* 19:423–443. doi:10.1146/annurev.cellbio.19.111401.091318
- Signor, D., K.P. Wedaman, J.T. Orozco, N.D. Dwyer, C.I. Bargmann, L.S. Rose, and J.M. Scholey. 1999. Role of a class DHC1b dynein in retrograde transport of IFT motors and IFT raft particles along cilia, but not dendrites, in chemosensory neurons of living *Caenorhabditis elegans*. *J. Cell Biol.* 147:519–530. doi:10.1083/jcb.147.3.519
- Sloboda, R.D., and L. Howard. 2007. Localization of EB1, IFT polypeptides, and kinesin-2 in *Chlamydomonas* flagellar axonemes via immunogold scanning electron microscopy. *Cell Motil. Cytoskeleton.* 64:446–460. doi:10.1002/cm.20195
- Walz, J., D. Typke, M. Nitsch, A.J. Koster, R. Hegerl, and W. Baumeister. 1997. Electron tomography of single ice-embedded macromolecules: three-dimensional alignment and classification. *J. Struct. Biol.* 120:387–395. doi:10.1006/jsbi.1997.3934